PROCEEDINGS, Thirty-Sixth Workshop on Geothermal Reservoir Engineering
Stanford University, Stanford, California, January 31 - February 2, 2011
SGP-TR-191

# COMPOSITIONAL FLOW SIMULATIONS OF MIXED $CO_2$-WATER INJECTION INTO GEOTHERMAL RESERVOIRS: GEOTHERMAL ENERGY COMBINED WITH $CO_2$ STORAGE

Hamidreza Salimi, Remco Groenenberg, and Karl-Heinz Wolf

Department of Geotechnology, Delft University of Technology
Stevinweg 1
Delft, 2628 CN, The Netherlands
e-mail: h.salimi@tudelft.nl

## ABSTRACT

The Delft Geothermal Project is a consortium of governmental and industrial partners that aims to develop an innovative geothermal system at the campus of Delft University of Technology (DUT). Annually, DUT consumes 11 million $m^3$ of gas, thus producing approximately 22000 tons of $CO_2$ of which 15000 tons are attributed to the generation of electricity. The planned geothermal system is designed to contribute up to 5 MW, which results in a $CO_2$ emission reduction of approximately 10000 tons. To reduce $CO_2$ emission further, a feasibility study is ongoing to also capture the $CO_2$ and coinject it with the cooled-down-return water of the geothermal system. In this way, synergy is established between geothermal energy production and subsurface $CO_2$ storage. To estimate the storage potential of the aquifer under Delft, and to assess the influence of coinjection of $CO_2$ on the performance of the geothermal system, we simulate mixed $CO_2$-water injection into the aquifer for various injected $CO_2$ concentrations, taking into account the spatial distribution of the fluvial sandstone bodies, their connectivity, and their internal permeability heterogeneity. For this purpose, we have applied a new and effective solution approach to deal with phase disappearance and appearance, called the "negative saturation" (NegSat) solution approach. In the NegSat solution approach, a single-phase multi-component fluid is replaced by an equivalent fictitious two-phase fluid with specific properties. The properties of the fictitious two-phase fluid are such that in the single-phase aqueous region, the extended saturation of the fictitious phase is negative. Our results show that as long as the injected $CO_2$ remains completely dissolved in the aqueous phase for the entire process, as the overall injected-$CO_2$ mole fraction increases, the useful energy extraction decreases slightly, but the maximum stored $CO_2$ increases accordingly. However, formation of a $CO_2$-rich phase changes the character of the solution in terms of useful energy production/$CO_2$ storage.

## INTRODUCTION

Concern about global warming is driving research and development aimed at reducing the emissions of greenhouse gases such as $CO_2$. One way of reducing $CO_2$ emissions is to partly replace conventional energy sources for heating buildings (e.g., cogeneration units) with geothermal energy. A further reduction could be achieved by capturing the remaining emitted $CO_2$ and to coinject it with the cooled-down-return water of the geothermal system. However, major issues such as how to estimate $CO_2$ breakthrough time, and the influence of coinjection of $CO_2$ on heat extraction remain poorly understood. In this paper, we use the simulation results of mixed $CO_2$-water injection for various injected $CO_2$ concentration to answer these questions.

Injection of $CO_2$ into geothermal reservoirs is a new research topic that emerged with the increased interest in geothermal energy production. Brown (2000) proposed a novel enhanced geothermal systems (EGS) concept that uses $CO_2$ instead of water as heat transmission fluid, and that achieves geologic sequestration of $CO_2$ as an ancillary benefit. Following up on his suggestion, Pruess (2006, 2008) evaluated the thermophysical properties and performed numerical simulations to explore the fluid dynamics and heat transfer issues in an engineered geothermal reservoir that would be operated with $CO_2$. In addition, Xu and Pruess (2010) performed chemically reactive transport modeling to investigate fluid-rock interactions in an EGS operated with $CO_2$. Our work differs from the mentioned works, because we do not use $CO_2$ as a working fluid, but we coinject $CO_2$ into a geothermal reservoir to store $CO_2$ simultaneously with hot-water extraction. We consider only capillary pressure and gravity, and also take into account longitudinal heat conduction with the porous rock. However, effects of salinity and reactions are not taken into account.

The aim of this paper is to investigate the influence of injected $CO_2$ concentrations on the efficiency of $CO_2$ sequestration in aquifers, and on heat extraction. First, we review the history and the framework of the Delft geothermal project. Then, we discuss the results of a study on the reservoir geology and petrophysics of the aquifer, from which we obtained the porosity and the distribution of permeability heterogeneities in the aquifer. After that, we briefly explain our novel negative saturation (NegSat) solution approach for non-isothermal compositional flow to deal with problems that involve phase appearances and disappearances. Subsequently, we give a set of simulation results that show the possible bifurcations of cold mixed $CO_2$-water injection into a geothermal reservoir. These results, which are plotted in a useful energy/storage capacity diagram, are discussed in detail. Finally, we summarize our findings in the conclusion section.

## HISTORY AND FRAMEWORK

In the preceding decade, hundreds of shallow heat-cold storage facilities were installed in The Netherlands for large office- and commercial buildings, and for heat pumps for houses and small commercial buildings. The energy thus provided ranges from circa 50 kW to 20.000 kW per facility (van Heekeren et al. 2005). During the past five years, production of deep geothermal energy began to develop, starting with two doublets for glasshouses in Bleiswijk (1700 m depth, circa 10MW) and one for heating houses in The Hague (2000 m depth). Both projects confirmed the presence of favorable geological conditions under the Western part of The Netherlands. A major part of the Mesozoic sub-surface consists of sedimentary rock with, at intervals, thick reservoir sands at depths in excess of 1500 m. The geothermal gradient varies from ca. 3ºC/100m to 4.5ºC/100m (van Wees et al. 2009).

Students of Delft University of Technology, Department of Geotechnology, initiated the Delft Geothermal Program (DAP). DAP started a feasibility study where innovation (casing drilling technology using composite materials, and optional $CO_2$ coinjection) is combined with the commercial production of geothermal energy for heating offices and student houses on the campus. Currently, the campus is powered by a 79 MW power plant, which holds two cogeneration units for base-load and three gas boilers for peak demand. Electricity generated by the plant is delivered through the “public” electricity grid; heat generated by the plant is delivered by a high-temperature heating grid.

The university plans to renovate its plant and high-temperature heating grid within the next ten years. One option is to transfer the latter to a low-temperature heating grid (70 °C in, 30 °C return). In addition, the municipality of Delft, local housing corporations, and an energy provider propose to develop a low-temperature heating grid for 22000 newly constructed and redeveloped buildings and houses. A feasibility study for a multi-purpose power plant for the campus (DAP, Wolf et al. 2008 ) made clear that a geothermal doublet must be located at or near the power plant on the campus to maximize the heat gain and minimize transport costs.

In 2009, the University was granted an exploration and production license for geothermal energy by the government. In this 60 $km^2$ licensed area, three projects are under development: two doublets for heating glass houses and public buildings and one for the combined geothermal/cogeneration power plant for the university (Fig. 1). Drilling of the four wells for the two doublets of the glasshouse farmers is almost completed. Subsurface information from these wells is and will be used to further improve the reservoir geological and petrophysical knowledge of the aquifers present under the licensed area. Drilling of the geothermal doublet on the campus of DUT is planned for the first quarter of 2012.

## RESERVOIR CHARACTERIZATION

The geothermal doublet will consist of two wells: a hot-water production well, and a cold-water reinjection well. The wells target the Delft Sandstone Member, a fluvial sandstone formation contained in a structural low at a depths ranging from 1.7 to 2.3 km below surface. The geothermal potential of this aquifer strongly depends on two key parameters: the temperature of the formation water in the aquifer (heat in place), and the permeability of the aquifer. Temperature of the formation water is a function of depth below surface. Bottomhole temperature readings indicate that the geothermal gradient in the area is approximately 3ºC/100m (Smits 2008), which results in a temperature estimate of 65-80 ºC for the formation water contained in the Delft Sandstone Member. This is sufficient for use in a low-temperature grid-heating network or glasshouse heating system. The second parameter to be estimated is the permeability of the aquifer, which directly influences the production (and reinjection) rate that can be reached. For this purpose, a reservoir characterization study of the Delft Sandstone Member was done to assess the spatial distribution of the fluvial sandstone bodies, their connectivity and their internal permeability heterogeneity. In this section, the results of this study and their implications for compositional flow simulations of cold $CO_2$-water injection into a geothermal reservoir are briefly elucidated.

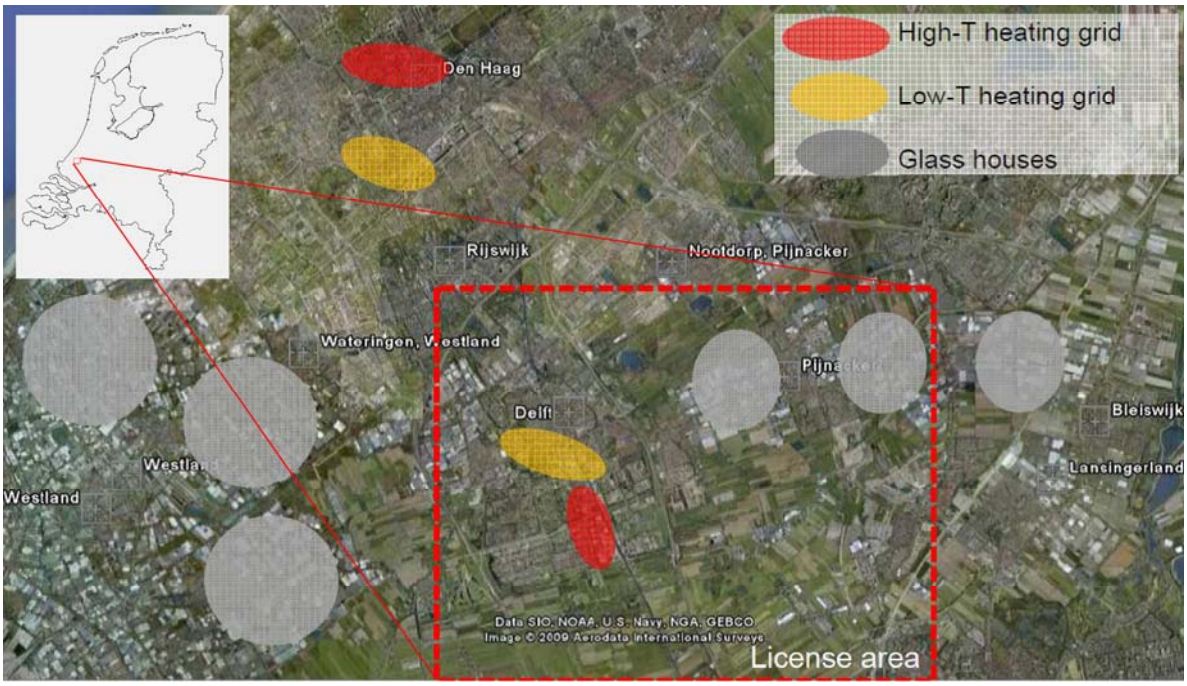


*Figure 1: Permitted geothermal production activities and different application within and around the Delft University Licensed area. Width of the image is 18 km.*

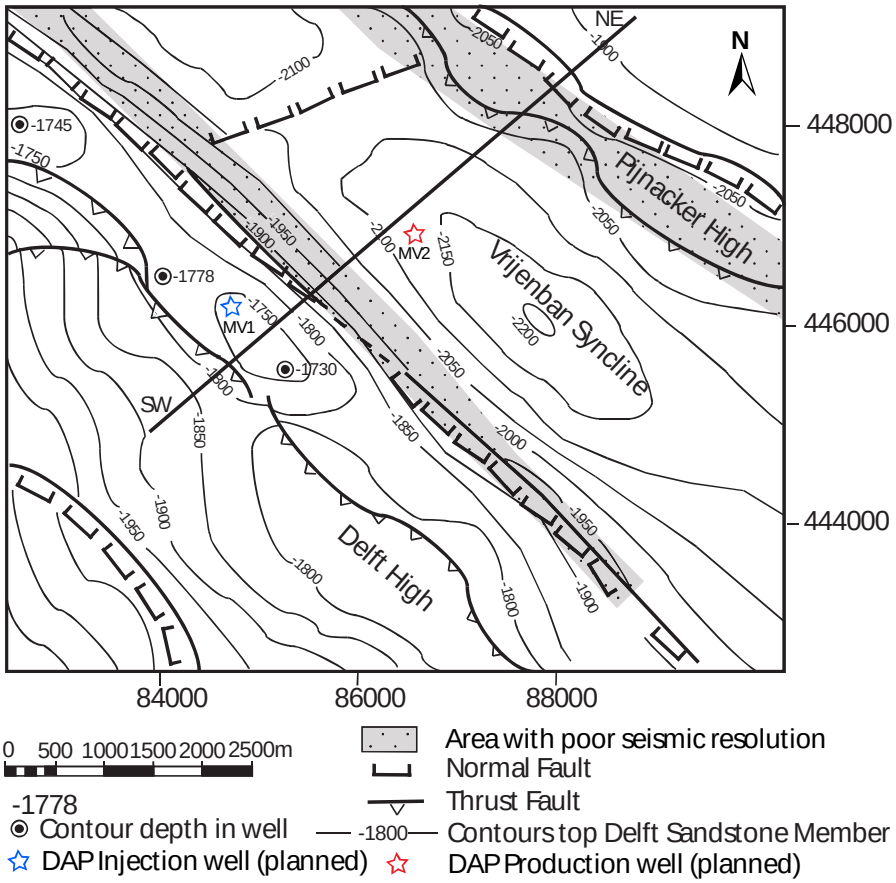


*Figure 2: Contour map of top of the Delft Sandstone Member with the main structural elements. Map is constructed from pre-stack depth-migrated seismic data and regional time seismic data. SW-NE line is location of seismic section in Fig. 3.*

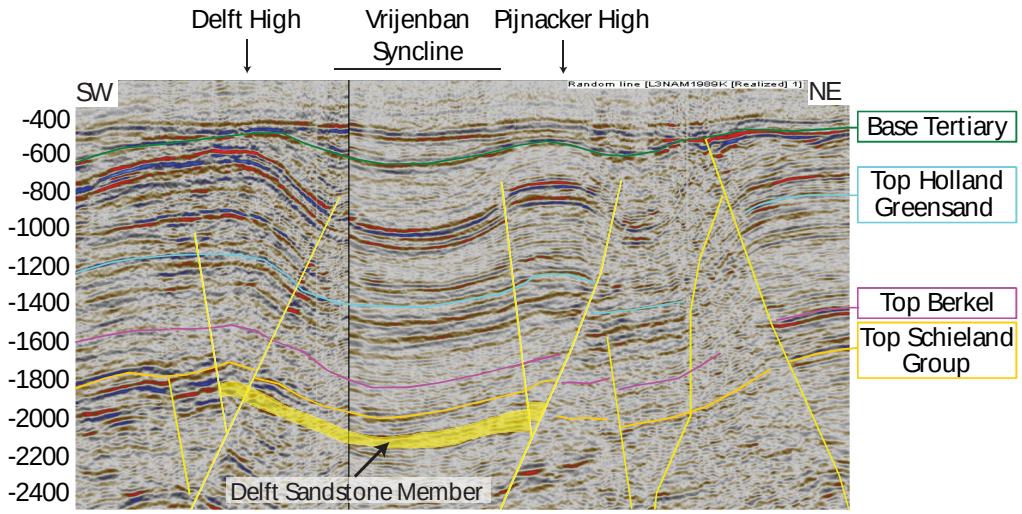


*Figure 3: Seismic cross-section (depth in m) through the study area, which shows that the Delft Sandstone Member sits in a gentle, broad syncline bounded by two pop-up structures (inverted normal faults), and has subtle thickness difference.*

## Reservoir Architecture

The Delft Sandstone Member is deposited in the western and central parts of the West Netherlands Basin. It is a light-grey, fine to coarse-gravelly, massive sandstone sequence with abundant lignitic matter, which varies in thickness between 0 (absent) and 130 m (Smits 2008). It is interpreted as stacked distributary-channel deposits in a lower coastal-plain setting (Van Adrichem Boogaert and Kouwe 1993). Based on core, well-log, and cuttings sample analysis, the Delft Sandstone Member is subdivided into three units with distinctly different gamma-ray signature, facies description, and depositional architecture: (1) a lower unit containing single-stacked, fining-upward meandering river sandstone bodies interbedded with floodplain deposits that formed in a period of relatively high rate of accommodation space increase related to tectonic activity in the WNB; (2) a middle unit containing floodplain deposits (silt- and claystones with coal layers) that formed during sea-level highstand (MFS); and (3) an upper unit containing multiple-stacked, laterally amalgamated fluvial channel sandstone bodies that formed in a period of relatively low accommodation space increase when the river was forced to migrate laterally and cannibalize its own deposits (Groenenberg et al. 2010).

## Reservoir Properties

Knowledge on the spatial variability in reservoir properties, such as porosity and permeability, is of primary importance in evaluating the flow of hot and cold water through formations. Appraisal drilling for hydrocarbons in and around the target area has indicated that the Delft Sandstone Member has promising reservoir qualities, i.e., high porosity and permeability. However, no additional information was available on their spatial and vertical variability. A core study on wells in the Moerkapelle oil field (12 km to the northeast), which was done in support of this reservoir characterization study (Drost and Korenromp 2009; Loerakker 2009), indicates that the three units identified in the Delft Sandstone Member have distinctly different porosities and permeabilities. In the lower unit (Unit 1), the average porosity is about 19% and the permeability increases from about 90 mD at the base to 295 mD at the top of the unit. In the upper unit (Unit 3), which contains significantly coarser-grained material than the lower unit, the average porosity is 30% and the permeability varies between 725 mD and 1130 mD. The middle unit (Unit 2), which consists of very fine-grained sediment, has an extremely low porosity and permeability. Average net sand content (N/G) in the Delft Sandstone Member in the wells is about 0.65. As such, results from these studies on the vertical distribution of porosity and permeability show that the Delft Sandstone Member has two units with good reservoir quality. However, vertical connectivity between the lower and upper unit is very likely impeded by the presence of Unit 2. Furthermore, based on the depositional model proposed in the previous section, it must be assumed that the lateral connectivity parallel to the basin axis is higher than perpendicular to it. Moreover, the lateral connectivity perpendicular to the basin axis is probably poor in Unit 1, which contains the isolated single-stacked channels. In contrast, in Unit 3, which contains the multiple-stacked channels, the lateral connectivity perpendicular to the basin axis is probably much higher.

A three-dimensional reservoir model (Petrel™) was constructed based on the available seismic data and well data of existing oil- and gas wells in the region.

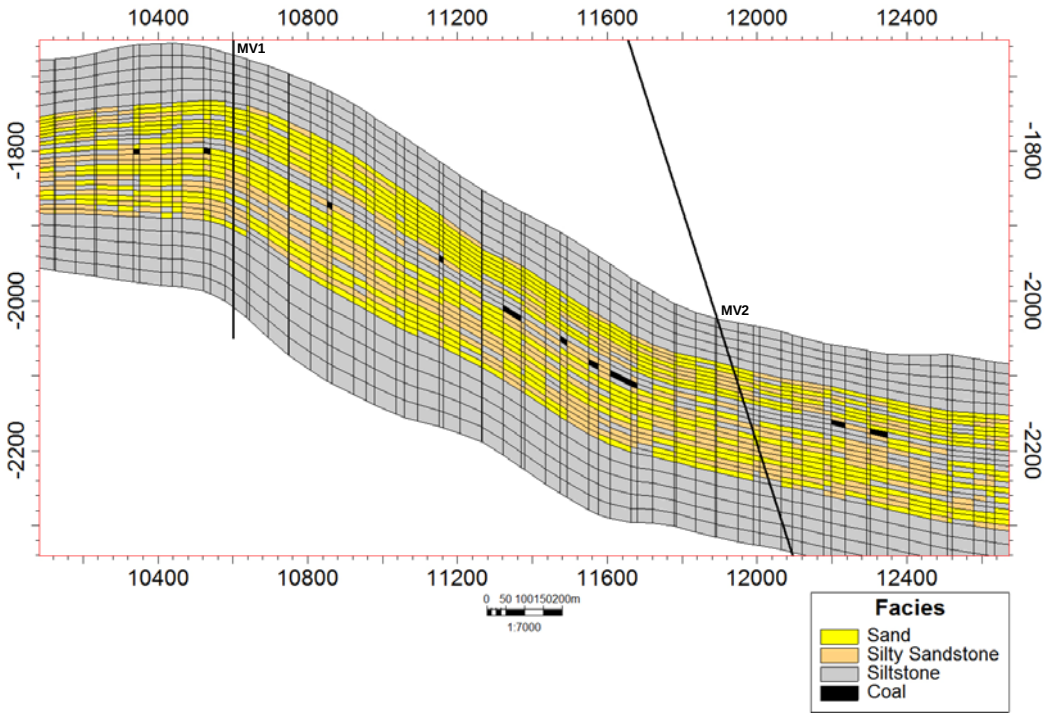


*Figure 4: Cross-section through the reservoir model between the planned injection well (MV1) and production well (MV2). Colors represent the type of sediment (facies) present in the cell (see legend).*

Object-based facies modeling was applied to fill in the space between the wells with different types of sediment. Based on the log, core, and cuttings analyses on the wells in the Delft and Moerkapelle oilfields (Drost and Korenromp 2009; Loerakker 2009), four different types of sediment were defined: sand, silty sandstone, siltstone, and coal. Each type has its own characteristic range of porosities and permeabilities attached to it, which were obtained from the core and cuttings analyses. Furthermore, object-based facies modeling requires input on the expected geometry of the fluvial sand bodies that is partly derived from the depositional setting, such as the direction and size of the meandering channel belt. Channel thickness is set as measured in cores, and varies from 1.5 to 4.5 m with an average of 3 m (Loerakker 2009). Channel width is derived from the thickness using the general equation developed by Fielding and Crane (1987), and varies from 12 to 195 m with an average of 92 m. Additional information governing the lateral distribution of the sand bodies, such as river sinuosity, meander wavelength, and amplitude, were obtained from literature on fluvial systems deposited under similar paleogeographical and paleoclimatic conditions, and with similar width/thickness characteristics. Fig. 4 displays a cross-section through the facies model between the planned injection and production well of the Delft geothermal doublet, which shows the level of heterogeneity in the Delft Sandstone Member.

## RESERVOIR SIMULATION

Many problems in enhanced oil recovery and $CO_2$ sequestration involve transitions between single-phase and two-phase regions (Pruess 2004; Chen et al. 2006). Different systems of equations describe the behavior in the single-phase and in the two-phase regions (Lake 1989; Chen et al. 2006). Consequently, primary variables for each phase-state region will be different. A location in the reservoir can stay either in the two-phase (saturated) state or in the single-phase (undersaturated or oversaturated) state. Furthermore, from the $l^{th}$ iteration to the $(l + 1)^{th}$ iteration in a Newton-Raphson (NR) procedure (Chen et al. 2006), the grid cell can stay in the same state or change to another phase state. Apart from the system of equations, also the thermodynamic conditions can vary in different phase states. Therefore, from the computational point of view, it is important to deal properly with the phase appearance and disappearance to obtain convergence of the NR procedure. The state of a reservoir can change from saturated to undersaturated (or oversaturated) or vice versa. Determination of a proper phase state during the state transition is called the bubble- or dew-point problem (hereinafter referred to as bubble point). If the bubble-point problem can be recognized promptly, and reasonable unknowns can be selected for different phase states of a reservoir, convergence of the NR procedure can be enhanced.

Conventional algorithms require a cumbersome procedure to switch between single-phase and two-phase behavior in a grid cell. The main problem is that in a sequence of NR convergence steps, consecutive iterations may switch from single-phase to two-phase or vice versa.

Recently, a new solution approach, called the "negative saturation approach" (NegSat), is introduced, which circumvents the use of cumbersome switches in isothermal reservoirs and does not require an additional equation. The NegSat solution approach was first introduced by Abadpour and Panfilov (2009) for isothermal flow without diffusion and by Panfilov and Rasoulzadeh (2010) for isothermal flow with diffusion. Salimi et al. (2011) have extended the NegSat solution approach to non-isothermal compositional flow. In this paper, we apply the non-isothermal NegSat solution approach to simulate cold mixed $CO_2$-water injection into a geothermal reservoir, because the non-isothermal characteristic of the flow plays a crucial role in geothermal reservoirs.

## Non-Isothermal Negative Saturation Approach

We formulate the NegSat solution approach for non-isothermal compositional two-phase flow. Our aim is to have a uniform system of equations for the entire reservoir that could properly deal with different phase states of the reservoir without changing the primary variables and thermodynamic-constraint conditions. For this purpose, we need to know beforehand how many phases could coexist at most. For cold mixed $CO_2$-water injection into a geothermal reservoir, two phases could coexist at most (viz., a $CO_2$-rich phase and a water-rich phase). Therefore, we replace the equations for single-phase regions (i.e., oversaturated and undersaturated) with the equations for equivalent fictitious two-phase regions with specific properties. We use the principle of equivalence to derive the specific properties. The governing equations consist of the species-balance equations, Darcy's law, the energy conservation equation, and the thermodynamic equilibrium between the two phases. A possible salinity of the water phase is not considered. Further details about the non-isothermal NegSat solution approach can be found in Salimi et al. (2011).

### *Specific Properties*

For two-phase regions, the fictitious two-phase flow equations remain the same as the classical two-phase flow equations. The principle of equivalence enables us to define expressions for all symbols of the fictitious two-phase flow so that they also describe the single-phase flow behavior. If we use these expressions, we convert two-phase flow equations to single-phase flow equations.

The principle of equivalence implies that first the undersaturated phase molar density must be equal to the total molar density of the fictitious two phases. Secondly, the overall concentration of component *i* in the undersaturated phase must be equal to that in the fictitious two phases. Thirdly, the undersaturated phase flux must be equated to the total flux of the fictitious two phases. From these implied equalities, we can derive specific properties for viscosity, relative permeabilities, pressures, and mass densities. Note that the capillary pressure $p_c$ becomes zero for the undersaturated phase. Finally, the energy conservation equation for the undersaturated phase must be equivalent to that for the fictitious two phases.

The saturation of the equivalent gas $\hat{S}_g$ is called the extended gas saturation, it reads

$$\hat{S}_g = \frac{z_i - x_{iw}}{x_{ig} - x_{iw}}, \quad i = 1, 2, ..., N_c. \tag{1}$$

In Eq. 1, $z_i$ is the overall mole fraction of component *i* and $x_{i\alpha}$ is the mole fraction of component *i* in phase $\alpha$. The extended gas saturation for the undersaturated state is negative (i.e., $\hat{S}_g < 0$). The reason is as follows. For light components (i.e., $x_{ig}/x_{iw} > 1$), the phase state of a system, for a given temperature *T* and pressure *P*, is undersaturated when $z_i < x_{iw}$. Therefore, the numerator of Eq. 1 is negative and the denominator of Eq. 1 is positive. As a result, the extended gas saturation $\hat{S}_g$ becomes negative. Also, for heavy components in a two-phase mixture (i.e., $x_{ig}/x_{iw} < 1$), the phase state of a system, for a given temperature *T* and pressure *P*, is undersaturated when $z_i > x_{iw}$. Hence, the numerator of Eq. 1 is now positive and the denominator of Eq. 1 now negative. As a result, the extended gas saturation (Eq. 1) again becomes negative. When the extended saturation is zero, the phase state of a system is at the bubble point. Further details about the negative-saturation solution approach can be found in Salimi et al. (2011).

## Numerical Model

We consider cold mixed $CO_2$-water injection into a geothermal reservoir modeled as a two-dimensional (2D) vertical porous medium initially filled with hot liquid water. In this model, we consider capillary pressure and gravity. We take into account longitudinal heat conduction with the porous rock, but, for illustration purposes, we avoid the complication of heat loss to the overburden and underburden.

Due to high pressures and temperatures, a $CO_2$-water mixture is a non-ideal mixture. Therefore, we use the Peng-Robinson-Stryjek-Vera equation of state with the Modified Huron-Vidal second-order mixing rule that uses the Non-Random Two-Liquid activity

coefficient model to determine the phase equilibrium for the non-ideal $CO_2$-water mixture. A volume-shift procedure is applied to obtain an accurate liquid density. Further details about the thermodynamic model can be found in Eftekhari et al. (2011). We take into account the density heterogeneity in Darcy's equation and the density variations in the accumulation term of the conservation equations.

We consider a geothermal reservoir with a length of 1500 m, a width of 1500 m, and a height of 60 m. Initially, the reservoir is saturated with hot water. In other words, the initial gas ($CO_2$) saturation in the geothermal reservoir is equal to zero. A cold mixture of $CO_2$-water is injected through the entire cross-area of the reservoir from the left side and, subsequently, water and $CO_2$ are produced through the entire cross-area of the reservoir at the opposite side. Table 1 shows the basic input data for the numerical simulations. The gas and liquid relative permeability functions used for obtaining the numerical solutions are

$$k_{rw} = (1 - S_g)^4, \quad \text{and} \quad k_{rg} = S_g^2(1 - (1 - S_g)^2). \qquad (2)$$

*Table 1: Data used in the numerical simulations.*

| | |
|---|---|
| Maximum injection pressure (bar) | 255 |
| Bottomhole production pressure (bar) | 205 |
| Initial Temperature (K) | 353.15 |
| Injection Temperature (K) | 293.15 |
| Maximum water-Injection rate ($m^3/s$) | 0.04167 |
| Rock grain density ($kg/m^3$) | 2650 |
| Rock specific heat capacity (J/kg/K) | 1000 |
| Total thermal conductivity (W/m/K) | 2.1 |
| Geometric mean permeability (mD) | 21.6 |
| Mean porosity | 0.17 |
| Residual water saturation | 0 |
| Residual gas saturation | 0 |
| Number of grid cells | 23×35 |

The reservoir properties of the aquifer correspond to those of the Delft sandstone member below Delft, as discussed earlier. Figs. 5 and 6 show the permeability and porosity distribution in the Delft Sandstone Member between the two planned wells. The viscosities of the liquid and gaseous phase are approximated by the viscosities of $CO_2$ and water as functions of temperature (Perry and Green 1997); they read

$$\mu_g = 1.6128\times10^{-3} - 9.0436\times10^{-6}T + 0.0135\times10^{-6}T^2 - 1.9476\times10^{-12}T^3, \qquad (3)$$

$$\mu_w = 2.414\times10^{-5}\times10^{(247.8/(T-140))}. \qquad (4)$$

In Eqs. 3 and 4, $T$ is the absolute temperature in Kelvin and the unit of viscosity is Pa·s. These equations disregard the compositional dependence.

To calculate the heat capacity of phase $\alpha$, we assume that the heat capacity of phase $\alpha$ is the sum of the molar heat capacities of its components, i.e., we disregard the energy of mixing. We use the following expressions for heat capacity of $CO_2$ and water (Perry and Green 1997):

$$C_{p,CO_2} = 45.369 + 8.6881\times10^{-3}T - 961930\times T^{-2}, \qquad (5)$$

$$C_{p,H_2O} = 276.37 - 2.0901\,T + 8.125\times10^{-3}T^2 - 0.014116\times10^{-3}T^3 + 9.3701\times10^{-9}T^4. \qquad (6)$$

Eqs. 5 and 6 express the heat capacity in the unit of (J/mol/K) and $T$ is the absolute temperature in Kelvin.

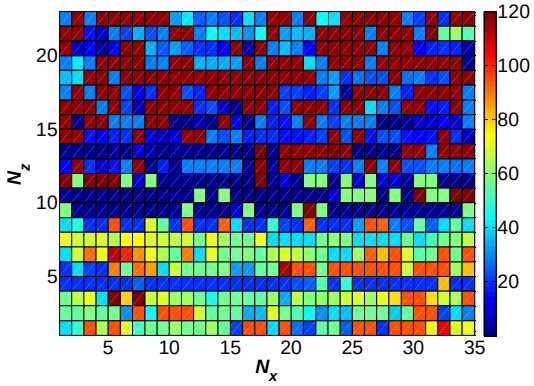


*Figure 5: Permeability distribution (mD) of the vertical x-z cross-section.*

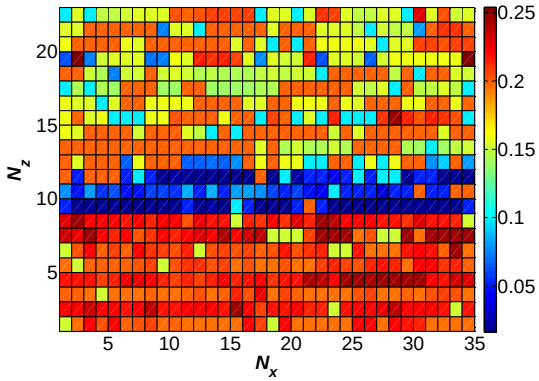


*Figure 6: Porosity distribution of the cross-section.*

We discretize the geothermal reservoir into 23×35 grid-cells in the $z$ and $x$ direction. The number of grid cells is the same as that used for the permeability and porosity distribution. For discretization in space, we use the implicit upwind finite-volume method on the cell-centered scheme. For each simulation case, the water-injection rate is uniform.

## RESULTS AND DISCUSSION

We illustrate the non-isothermal NegSat solution approach by way of example to cold mixed $CO_2$-water injection into a geothermal reservoir. In the

simulations, we vary the overall mole fraction of $CO_2$ injected and the properties of the 2D reservoir. Based on the possible phase states for $CO_2$-water injection into a geothermal reservoir, we investigate two cases in terms of the overall mole fraction of $CO_2$ injected. To emphasize the effect of heterogeneity of the medium, we compare the results of a heterogeneous case with the results of a uniform case. In all cases, we continue to inject cold mixed $CO_2$-water into the reservoir and produce hot water until either $CO_2$ breakthrough or cold-water breakthrough (for pure cold-water injection) happens. Moreover, the initial target mode for the injection well is the uniform water-injection rate. However, a maximum bottomhole pressure of 255 bar acts as a constraint for the injection well. Therefore, if the bottomhole pressure of the injection well exceeds 255 bar during the simulation, the maximum bottomhole pressure becomes the target mode for the injection well and the injection rate is reduced accordingly.

The results are organized as follows. First, we examine the first heterogeneous case. Then, we compare the results of the first heterogeneous case with the results of the uniform case for the same overall injected-$CO_2$ mole fraction. After that, we illustrate the second heterogeneous case, based on which we discuss the influence of various $CO_2$ injection fractions on the storage/production mechanisms of $CO_2$ and on production of hot water from the geothermal reservoir. Finally, we provide a plot of useful energy (exergy) extraction versus stored $CO_2$ as a screening method for optimal geothermal recovery and/or maximal storage of $CO_2$.

**Case 1**

Case 1 has an overall injected-$CO_2$ mole fraction of 0.02 (or about 49.9 kg of $CO_2$ per ton of water at room conditions). Fig. 7a shows the extended-gas-($CO_2$)-saturation profiles at $t$ = 30 yr for this case. The extended gas saturation is below zero for the entire time span considered, indicating that all the injected $CO_2$ is completely dissolved in the aqueous phase. Fig. 7a thus essentially displays a single-phase displacement process in the entire domain. The negative values of the extended saturation indicate how far the phase state of the reservoir is from a two-phase state. Note that when the extended gas saturation becomes equal to zero, the phase state of the reservoir would be at the bubble-point state. Fig. 7a clearly reveals that the saturation pattern is strongly influenced by the permeability and porosity distribution of the reservoir. Fig. 7b shows the temperature profiles at $t$ = 30 yr for case 1. Evidently, the temperature pattern is not affected by heterogeneity as opposed to the extended-gas-saturation pattern. By combining the temperature profile with the extended-gas-saturation profile, we obtain the corresponding overall-$CO_2$-mole-fraction profile, which is shown in Fig. 7c. As can be seen in Fig. 7c, $CO_2$ breakthrough has already occurred before 30 years. Furthermore, the $CO_2$ composition decreases monotonically from the injected $CO_2$ mole fraction (0.02) at the injection side to the initial $CO_2$ mole fraction (0) at the production side.

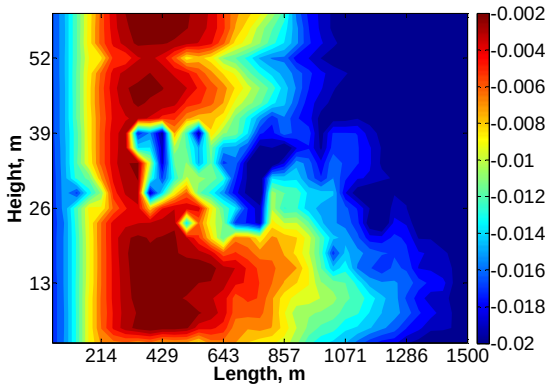


*Figure 7a: Extended-gas-saturation pattern at t = 30 yr for case 1.*

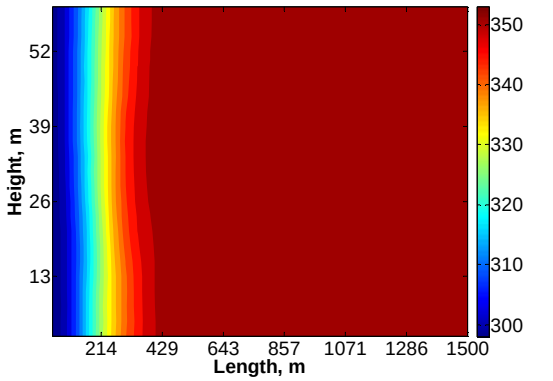


*Figure 7b: Temperature pattern (in K) at t = 30 yr for case 1.*

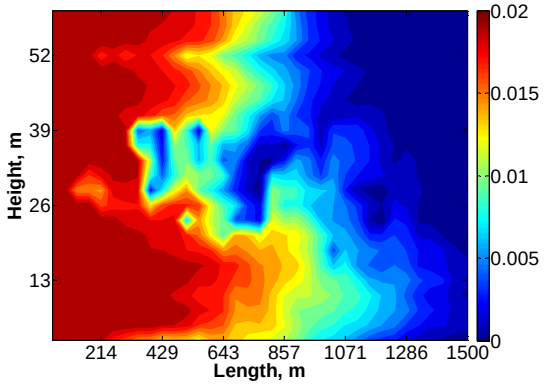


*Figure 7c: Overall-CO2-mole-fraction pattern at t = 30 yr for case 1.*

We note that the compositional front in Fig. 7c is far ahead of the thermal front in Fig. 7b, because the ratio of the composition wave to the thermal wave in this single-phase displacement example would be

$$\frac{v_c}{v_{th}} = \frac{(1-\varphi)(\rho c)_s}{\varphi(\rho c)_l} + 1 >> 1, \qquad (7)$$

where $v_c$ and $v_{th}$ are the speeds of the composition wave and thermal wave respectively, $\varphi$ is the porosity, $(\rho c)$ is the heat capacity per unit volume, and the subscripts $s$ and $l$ denote the solid and the liquid, respectively.

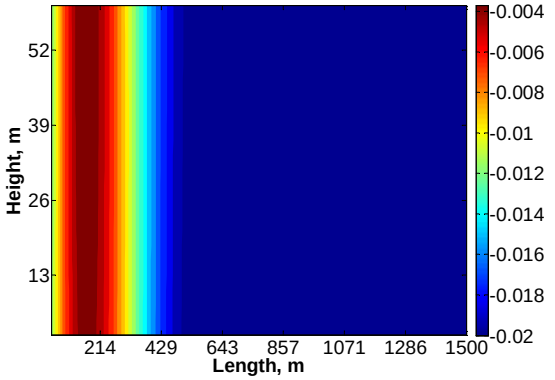


*Figure 8a: Extended-gas-saturation pattern at t = 30 yr for case 2.*

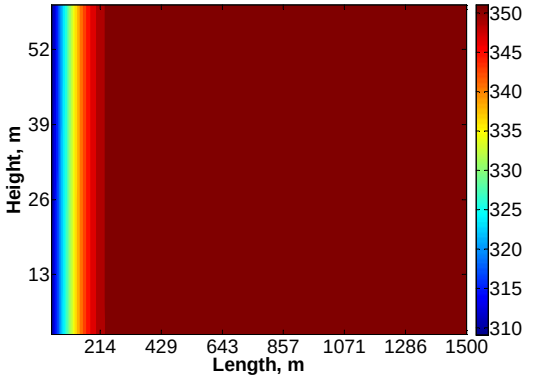


*Figure 8b: Temperature pattern (in K) at t = 30 yr for case 2.*

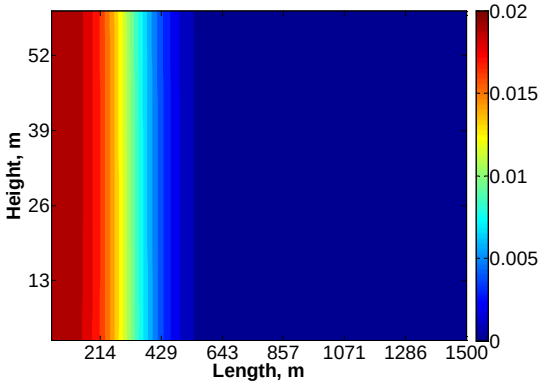


*Figure 8c: Overall-$CO_2$-mole-fraction pattern at t = 30 yr for case 2.*

**Case 2**

Case 2 also has an overall injected-$CO_2$ mole fraction of 0.02 (i.e., the same as that in case 1), but with a uniform permeability and porosity field. The uniform permeability is the geometric mean of the heterogeneous permeability field shown in Fig. 5, and the uniform porosity is the arithmetic mean of the heterogeneous porosity field shown in Fig. 6.

Fig. 8a shows the extended-gas-saturation pattern at $t$ = 30 yr for case 2. The extended gas saturation is below zero both at the injection side and at the production side, indicating single-phase aqueous regions. Fig. 8b displays the temperature pattern at $t$ = 30 yr for this case. Fig. 8c represents the corresponding overall-$CO_2$-mole-fraction pattern at $t$ = 30 yr. Moreover, Fig. 4c reveals that $CO_2$ breakthrough has not yet occurred at $t$ = 30 yr.

We compare the results of case 1 with the results of case 2 in Fig. 9 where the cumulative useful energy extraction (left $y$-axes) and the cumulative stored $CO_2$ (right y-axes) are plotted versus time for both cases. Fig. 9 shows that the rate of heat extraction and $CO_2$ storage of case 1 is higher than that of case 2 by a factor of 2.5. The reason for this observation is that in case 1, due to permeability variation at the injection side, the injectivity index is larger than the injectivity index of case 2 where the uniform permeability is used. As a result, more mixed $CO_2$-water is injected in case 1 for the same period. However, the maximum amount of cumulative heat extraction and $CO_2$ storage in case 2 are larger than in case 1. This is attributed to the characteristics of the heterogeneous permeability and porosity field used in case 1, i.e., the highly permeable zones cause $CO_2$ to bypass the less permeable zones, leading to earlier $CO_2$ breakthrough and shorter life time.

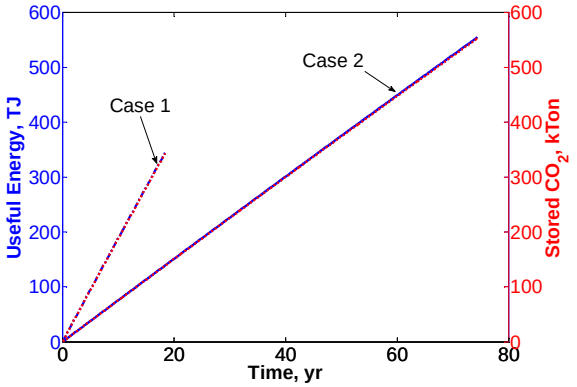


*Figure 9: Cumulative useful energy (exergy) extraction and stored $CO_2$ vs. time for cases 1 and 2.*

**Case 3**

Case 3 has an overall injected-$CO_2$ mole fraction of 0.03. Fig. 10a shows the extended-gas-($CO_2$)-saturation profiles at $t$ = 30 yr for this case. The extended gas saturation is below zero at the initial reservoir condition, indicating single-phase aqueous regions. However, close to the injection side, we observe $CO_2$ banks (high gaseous saturation values) at which the extended gas saturation is above zero, indicating two-phase regions. Therefore, there are three regions in terms of the phase state: (1) a single-phase region of an aqueous phase, (2) a two-phase region (i.e., $\hat{S}_g > 0$) with a gas phase with mainly supercritical $CO_2$ and an aqueous phase with mainly water, and (3) a two-phase region of a subcooled (liquid) $CO_2$-rich phase and an aqueous phase. Therefore, gas-phase appearance and a phase transition from subcooled $CO_2$ to supercritical $CO_2$ take place in this case.

Moreover, Fig. 10a illustrates that the $CO_2$ banks form at the highly permeable zones of the reservoir (see Fig. 5). This behavior reflects the changes in $CO_2$ solubility. The solubility of $CO_2$ in water decreases with an increase in temperature and a decrease in pressure. In highly permeable zones, the pressure is smaller than that in less permeable zones for a given Darcy velocity. As mentioned earlier, the speed of the composition wave is larger than the speed of the temperature wave. As a result, a part of the injected $CO_2$ dissolved in the aqueous phase reaches earlier the highly permeable zones that initially contain hot water. Therefore, the solubility of $CO_2$ reduces more in the highly permeable zones and consequently, a $CO_2$-rich phase forms that accumulates until local thermodynamic equilibrium is attained.

Figs. 10b and 10c display the temperature and corresponding overall-$CO_2$-mole-fraction profiles at $t$ = 30 yr. Fig. 10c reveals that $CO_2$ breakthrough has not yet occurred at $t$ = 30 years, and that the $CO_2$ concentration is not monotonically decreasing from the injection side towards the production side as opposed to cases 1 and 2. Indeed, the values of the overall $CO_2$ mole fraction in the banks are larger than the overall injected-$CO_2$ mole fraction. This is because of formation of a gas phase with mainly supercritical (subcritical) $CO_2$.

**Heat Recovery versus $CO_2$ Storage**

Fig. 11 plots the useful energy (exergy; De Swaan Aarons et al. 2004) at the end of the process (heat extraction) versus the maximum amount of stored $CO_2$ for various overall injected-$CO_2$ mole fractions. These are the salient characteristics of mixed $CO_2$-water injection into a geothermal reservoir. With no added $CO_2$, the criterion to end the project is at cold-water breakthrough. If a tiny amount of $CO_2$ is added, the criterion to end the project is when $CO_2$, dissolved in the aqueous phase, breaks through.

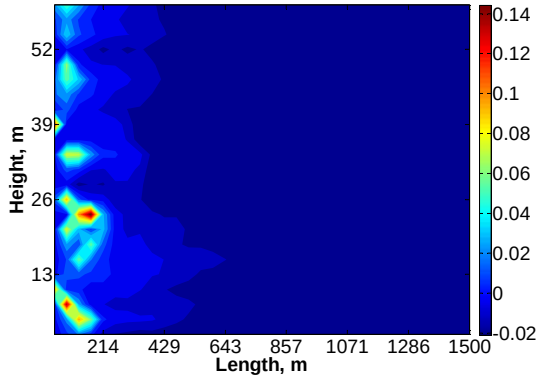


*Figure 10a: Extended-gas-saturation pattern at t = 30 yr for case 3.*

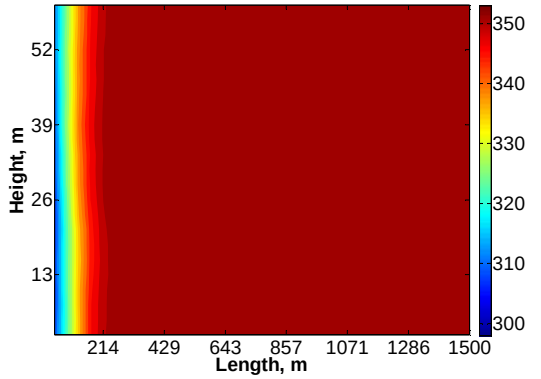


*Figure 10b: Temperature pattern (in K) at t = 30 yr for case 3.*

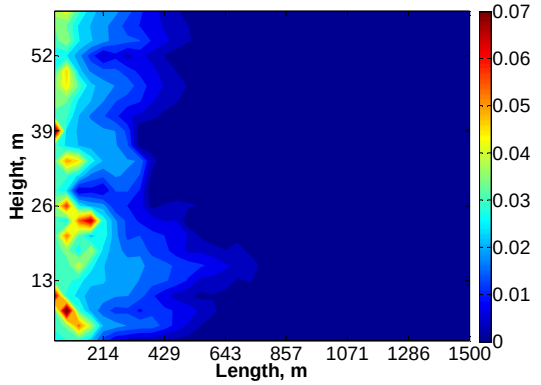


*Figure 10c: Overall-$CO_2$-mole-fraction pattern at t = 30 yr for case 3.*

We distinguish five trends in terms of useful energy/stored $CO_2$: trend 1 point no $CO_2$, trend 2 from point $z$ = 0.002 heterogeneous to point $z$ = 0.02 heterogeneous, trend 3 from point $z$ = 0.02 heterogeneous to point $z$ = 0.03 heterogeneous, trend 4 from point $z$ = 0.03 heterogeneous to point $z$ = 0.04 heterogeneous, and trend 5 from point $z$ = 0.02 uniform to point $z$ = 0.03 uniform. Trend 1

corresponds to cold-water injection (i.e., no $CO_2$); as a result, it is located on the *y*-axis. Consequently, there is a discontinuous change in terms of heat extraction (useful energy) from 1565 TJ to 417 TJ (1 T = $10^{12}$). In trend 2, as the overall injected-$CO_2$ mole fraction increases, the useful energy decreases slightly (17%), but the maximum stored $CO_2$ increases significantly. In trend 2, there is only an aqueous phase, i.e., single-phase displacement. In trend 3, a $CO_2$-rich phase forms that leads to increase of both the useful energy and the stored $CO_2$. Note that for the overall injected-$CO_2$ mole fraction of 0.03, there is one phase (aqueous phase) at the injection well. As the overall injected-$CO_2$ mole fraction becomes higher than 0.03, there are two phases at the injection well. Two-phase injection will change the characteristics of the process in terms of useful energy/stored $CO_2$, because trend 3 changes to trend 4 in which an increase in the injected $CO_2$ concentration reduces both the useful energy and the stored $CO_2$. Trend 5 corresponds to the uniform cases. In trend 5, as the overall injected mole fraction increases by a factor of 1.5, the useful energy remains approximately constant and the stored $CO_2$ increases by a factor of 1.45. The behavior of trend 5 (uniform case) is different from the behavior of trend 3 (heterogeneous cases) for the same range of the injected $CO_2$ concentration.

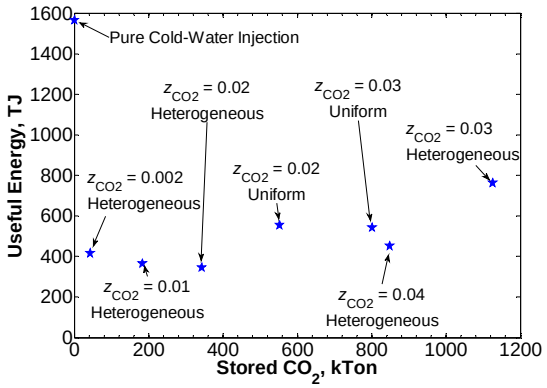


*Figure 11: Useful energy (exergy) extraction versus stored $CO_2$ at $CO_2$ breakthrough either in the aqueous or in the gaseous phase.*

Fig. 11 demonstrates that formation of a $CO_2$-rich phase will lead to a larger $CO_2$ storage capacity. This counterintuitive result is the consequence of the decrease in phase density of $CO_2$ as the $CO_2$-rich phase forms. This has three effects. First, the volume occupied by the injected $CO_2$ is larger in the gaseous phase. Thus, the $CO_2$ will necessarily come into contact with a larger volume of water, increasing the amount of $CO_2$ dissolved into water. Secondly, the larger density difference between the aqueous phase and the $CO_2$-rich phase at higher temperature causes the $CO_2$-rich phase to travel more rapidly, thereby mixing with more water as it moves upward while the aqueous phase moves downward by countercurrent flow (see also Kumar et al. 2005). Thirdly, the gaseous $CO_2$ banks in the highly permeable zones are surrounded by the less permeable zones. Therefore, the gaseous $CO_2$ banks will be trapped for a while until they are pressurized, after which they will be able to pass through the less permeable zones, which in turn, delays $CO_2$ breakthrough. However, in uniform cases, the $CO_2$-rich phase migrates to the top part of the reservoir from where it flows along the top seal to the injection well, leading to less $CO_2$ storage compared to the heterogeneous cases. These three effects lead to more $CO_2$ being stored in the geothermal reservoir as the $CO_2$-rich phase forms.

## CONCLUSIONS

- We extend the isothermal NegSat solution approach to non-isothermal conditions. This allows us to simulate cold $CO_2$-water injection into a geothermal reservoir without having to use switches such as is commonly done in the standard solution technique.
- Permeability and porosity heterogeneities in a geothermal aquifer significantly influence both heat extraction and $CO_2$ storage. Hence, reservoir characterization plays an important role in assessing the benefit of $CO_2$ storage and energy extraction.
- Increasing the amount of $CO_2$ in the injection mixture leads to bifurcation points at which the character of the solution changes.
- At low $CO_2$ injection concentrations (mole fraction below 2%, e.g., case 1), there is only a single-phase aqueous region. At mole fractions larger than 2% (case 3), gaseous $CO_2$ banks in highly permeable zones develop.
- A small amount of injected $CO_2$ will reduce the maximum amount of heat extraction significantly because $CO_2$ breakthrough always occurs earlier than cold-water breakthrough. However, increasing the amount of injected $CO_2$ will not always reduce the maximum amount of heat extraction and $CO_2$ storage monotonically. Particularly in heterogeneous cases, formation of a $CO_2$-rich phase leads to a larger amount of heat extraction and $CO_2$ storage compared to a case where all the injected $CO_2$ is dissolved into an aqueous phase.
- The behavior of the heterogeneous cases is different from the behavior of the uniform cases.

## ACKNOWLEDGEMENTS

This work has been performed within the framework of the Dutch National $CO_2$-storage program CATO-2, workpackage 3.5 and 3.2. We thank the Nederlandse Aardolie Maatschappij (NAM) for access to core and cuttings, PanTerra Geoconsultants for assistance with the cuttings analysis, and Schlumberger Information

Services for the use of the Petrel Seismic to Simulation software suite.

## REFERENCES


Abadpour, A. and Panfilov, M. (2009), "Method of negative saturations for modeling two-phase compositional flow with oversaturated zones," *Transport in Porous Media*, **79** (2), 197–214.

Brown, D. (2000), "A Hot Dry Rock Geothermal Energy Concept Utilizing Supercritical $CO_2$ Instead of Water," Conference paper presented at the Twenty-Fifth Workshop on Geothermal Reservoir Engineering, Stanford University, 233–238.

Chen, Z., Huan, G., Ma, Y. (2006), "Computational Methods for Multiphase Flows in Porous Media. Society for Industrial and Applied Mathematics, Philadelphia.

De Swaan Arons, J., Van der Kooi, H., Sankaranarayanan, K. (2004), "Efficiency and Sustainability in the Energy and Chemical Industries," ISBN 0824708458, Marcel Dekker Inc., New York.

Den Hartog Jager, D.G., (1996), "Fluviomarine sequences in the Lower Cretaceous of the West Netherlands Basin: correlation and seismic expression," In H.E. Rondeel, D.A.J. Batjes, and W.H. Nieuwenhuijs, eds., Geology of Gas and Oil under the Netherlands: Dordrecht, Kluwer Academic Publishers, 229–241.

Drost, G.I.A. and Korenromp, M.H.A. (2009), "Sediment-petrographical analysis of the Delft Sandstone," BSc. thesis, Delft University of Technology, Delft, the Netherlands.

Eftekhari, A.A., Bruining, J., Wahanik, H., Marchesin, D. (2011), "$CO_2$ injection in sub-salt water layers at 7000 m depth," Paper SPE 142191 to be presented at the SPE Reservoir Simulation Symposium, The Woodlands, Texas, USA, 21–23 February.

Gilding, D.T. (2010), "Heterogeneity determination of the Delft subsurface for heat flow modeling," MS thesis, Delft University of Technology, Delft, The Netherlands.

Gilding, D. T., Wolf, K-H A.A., Wever, A.K.T. (2010), "Integrating Multi Purpose Geothermal Systems with Local City Heating Grids," Conference paper presented at the World Geothermal Congress, Bali, Indonesia, 25–29 April, 1–9.

Groenenberg, R.M., Gilding, D.T., Donselaar, M.E., Drost, G.I.A., Korenromp, M.H.A., Loerakker, M., Wiggers, C.J.I., Wever, A.K.T., Wolf, K.A.A. (2010), "Targeting for geothermal energy production: Reservoir characterization and geothermal potential of the Delft Sandstone," Conference paper presented at the 72th EAGE Conference and Exhibition, Barcelona, Spain, 3814–3818.

Kumar, A., Ozah, R., Noh, M., Pope, G.A., Bryant, S., Sepehrnoori, K., Lake, L.W. (2005), "Reservoir Simulation of $CO_2$ Storage in Deep Saline Aquifers," *SPE Journal*, **10** (3), 336–348.

Lake, L.W. (1989), "Enhanced Oil Recovery," Englewood Cliffs, New Jersey: Prentice Hall.

Loerakker, M. (2009), "A core study to determine the heterogeneities in the Delft Sandstone Member in the Moerkapelle field," BSc. thesis, Delft University of Technology, Delft, the Netherlands.

Panfilov, M. and Rasoulzadeh, M. (2010), "Interfaces of phase transition and disappearance and method of negative saturation for compositional flow with diffusion and capillarity in porous media," *Transport in Porous Media*, **83** (1), 73–98.

Perry, R.H. and Green, D.W. (1997), "Perry's Chemical Engineers," Handbook–7th ed. McGraw-Hill.

Pruess, K. (2004), "Numerical simulation of $CO_2$ leakage from a geologic disposal reservoir, including transitions from super- to subcritical conditions, and boiling of liquid $CO_2$," *SPE Journal*, **9** (2), 237–248.

Pruess, K. (2006), "Enhanced geothermal systems (EGS) using $CO_2$ as working fluid—A novel approach for generating renewable energy with simultaneous sequestration of carbon," *Geothermics*, **35,** 351–367.

Pruess, K. (2008), "On production behavior of enhanced geothermal systems with $CO_2$ as working fluid," *Energy Conversion and Management*, **49**, 1446–1454.

Salimi, H., Wolf, K-H., Bruining, J. (2011), "Negative Saturation Approach for Compositional Flow Simulations of Mixed $CO_2$-Water Injection into Geothermal Reservoirs, Including Phase Transition and Disappearance," Paper SPE 142924 to be presented at the SPE EUROPEC/EAGE Annual Conference and Exhibition held in Vienna, Austria, 23–26 May.

Smits, P. (2008), "Construction of an integrated reservoir model using the Moerkapelle field for geothermal development of the Delft sandstone," MS thesis, Delft University of Technology, Delft, the Netherlands.

Van Adrichem Boogaert, H.A. and Kouwe, W.F.P. (1993), "Stratigraphic nomenclature of the

Netherlands, revise and update by Rijks Geologische Dienst (RGD) and Netherlands Oil and Gas Exploration and Production Association (NOGEPA)". Mededelingen Rijks Geologische Dienst 50.

Van Balen, R.T., van Bergen, F., de Leeuw, C., Pagnier, H., Simmelink, H., van Wees, J.D., Verweij, J.M. (2000), "Modeling the evolution of hydrocarbon systems of the inverted West Netherlands Basin, The Netherlands," *Journal of Geochemical exploration*, **69-70,** 685–688.

Van Heekeren, V., Snijders, A. L., Harms, H. J. (2005), "The Netherlands Country Update on Geothermal Energy," Conference paper presented at the World Geothermal Congress, Antalya, Turkey.

Van Wees, J-D., Kramers, L., Kronimus, A., Mijnlieff, H., Juez-Larré, J., Bonté, D., van Gessel, S., Obdam, A., Verweij, H. (2009), "Geothermal Energy in the Netherlands," Conference paper presented at the AAPG European Region Annual Conference, Paris-Malmaison, France, 23-24 November, 141–144.

Wolf, K.-H.A.A., Willemsen, A., Bakker, T.W., Wever, A.K.T., Gilding, D.T. (2008), "The Development of a Multi-purpose Geothermal Site in an Urban Area," Conference paper presented at the SPE-70th EAGE Conference and Exhibition, Rome, Italy, 1018–1022.

Wong, Th. E. (2007), "Jurassic". In Th. E. Wong, D.A.J. Batjes, and J. De Jager, eds., Geology of the Netherlands: Amsterdam, Royal Netherlands Academy of Arts and Sciences, 107–125.

Xu, T. and Pruess, K. (2010), "Reactive Transport Modeling to Study Fluid-Rock Interactions in Enhanced Geothermal Systems (EGS) with $CO_2$ as Working Fluid," Conference paper presented at the World Geothermal Congress 2010, Bali, Indonesia, 25-29 April.